LAWRENCE
LIVERMORE
NATIONAL
LABORATORY

LLNL-JRNL-618473

Modeling of Laser Interactions with composite Materials

A. Rubenchik, C. Boley

February 13, 2013

Applied Optics

Disclaimer

This document was prepared as an account of work sponsored by an agency of the United States government. Neither the United States government nor Lawrence Livermore National Security, LLC, nor any of their employees makes any warranty, expressed or implied, or assumes any legal liability or responsibility for the accuracy, completeness, or usefulness of any information, apparatus, product, or process disclosed, or represents that its use would not infringe privately owned rights. Reference herein to any specific commercial product, process, or service by trade name, trademark, manufacturer, or otherwise does not necessarily constitute or imply its endorsement, recommendation, or favoring by the United States government or Lawrence Livermore National Security, LLC. The views and opinions of authors expressed herein do not necessarily state or reflect those of the United States government or Lawrence Livermore National Security, LLC, and shall not be used for advertising or product endorsement purposes.

Modeling of Laser Interactions with Composite Materials

Charles D. Boley[1] and Alexander M. Rubenchik[1,*]

[1]*Lawrence Livermore National Laboratory, Livermore CA 94550*

[*]*Corresponding author: rubenchik1@llnl.gov*

We develop a microscopic model of laser interactions with composite materials consisting of fibers embedded within a matrix. A ray-trace model is shown to determine the absorptivity, absorption depth, and optical-power enhancement within the material, as well as the angular distribution of the reflected light. We also link the microscopic model with a macroscopic average description, which provides physical insight and overall results. We show that the parameters in this average model can be determined from the ray-trace calculations.

OCIS codes: 080.2710, 080.5692,160.2290, 290.7050.

1. Introduction

As composite materials become increasingly common in industry, their laser interactions are attracting attention. We are concerned here with a composite consisting of fibers embedded in epoxy. In contrast with the situation in a metal, in dielectrics light can penetrate appreciably into the material, since the absorption length is determined by the particular materials and material structure. Furthermore, since the scattering length is typically shorter than the absorption length, light undergoes multiple scatterings before absorption. A direct measurement of the absorptivity is difficult and depends on the material structure, see e.g. [1]. The optical properties of the fibers and epoxy are well known. We develop a ray-trace model which determines the material absorptivity from first principles, in terms of the refractive indices of the components and their geometry. It also determines the absorption depth and other important quantities such as the enhancement of optical power within the material. We are able to calculate the intensity and angular distribution of the reflected light.

The propagation of light in translucent materials with large absorption length can be described in terms of macroscopic models which are convenient for modeling [2,3]. Even the simplest two-flux model provides a good description of practical problems [4]. Typically, the parameters involved in this description are determined from specialized experiments. We will demonstrate that these parameters can be determined from our first-principles ray-tracing calculations.

We consider the specific cases of two composite materials, one with carbon fibers, and one with fused silica fibers. These have quite different optical properties, and their laser

interactions will turn out to be correspondingly different. We also restrict ourselves to consideration of normal incidence. The generalization of the model to more complex fiber geometry and the presence of nanoparticles is straightforward.

In each case, we determine the macroscopic optical quantities by performing ray-tracing simulations of successive Fresnel reflections and refractions within the material. While the greatest interest pertains to the diode wavelength of 0.8 μm, in the case of the carbon-fiber composite we also consider a range of wavelengths, varying from 0.5 μm to 4 μm. We obtain the specular and Lambertian components of the scattered light, which can be observed experimentally. Finally, in each case we show that the optical energy density becomes locally enhanced within the material, and we display the overall distribution.

To establish a connection between the macroscopic description and the microscopic modeling, we consider a finite slab of translucent material. The transmission and reflection coefficients can be calculated in terms of the averaged model parameters, and comparison with ray tracing results determines their values. Then we compare the calculation of the spatial intensity distribution from the ray tracing and the average modeling. We find reasonable agreement in the two approaches.

In conclusion, we discuss the applicability of the method to a variety of other situations.

2. Optical Model

We are concerned with composite materials containing a matrix of fibers (either carbon or fused silica) embedded in epoxy. Typically, the volume of the fibers is between 40% and 60% of the total volume. The diameter of a fiber is typically between 10 and 30 microns, thus large in comparison with the wavelength of light. The typical thickness of a ply is several hundred microns. Our model applies to a single ply, within which all fibers are assumed to have the same orientation. The neighboring ply (beneath this one) may have a different orientation.

The model can be naturally generalized to more complex geometries -- multi-ply structures with different plies orientation, different weaving patterns, and so forth.

A schematic cross section of the geometry is depicted in Fig. 1, which shows a laser beam incident on the surface of a ply. Embedded in the overall epoxy are several rows of fibers, running parallel to the surface. The fibers, seen in cross section, are modeled as identical cylinders extending parallel to one another into the paper. Here their nominal radius is $a = 5$ μm. In setting up our model, we first arranged the fibers in regular rows. We then translated the rows, parallel to one another, by random amounts. Finally, we randomly perturbed the positions of the individual fibers. Each run involved a new set of randomizations. The results are not very sensitive to the positions of the fibers. We expect the results to vary somewhat with the relative volumes (areas, in our model) of fibers and epoxy. Here we present results for the case of 50/50 fiber/epoxy areas. In order to simulate a large spatial extent parallel to the surface, fictitious mirrors are placed within the epoxy near the edges of the incoming beam (Fig. 1).

Since the fiber diameter is much larger than the wavelength of light, we utilize ray-tracing [5] to model the laser-composite interaction. In this approximation the results are independent of the fiber radius and are sensitive to the ratio of fibers/epoxy volume. The laser rays are normally incident upon the surface, with the electric field either parallel to the fibers (s-polarized) or perpendicular to the fibers (p-polarized). Because of the assumed planar geometry, the polarization remains s or p throughout the scatterings.

When the incoming beam encounters the surface of the epoxy, a fraction of the power is Fresnel-reflected. We take the real part of the epoxy index of refraction to be $n_{e,r} = 1.6$, independent of wavelength. This can differ by a few percent from material to material. Neglecting for the moment the imaginary part, which is a few orders of magnitude smaller, we thus have for the surface reflectivity of the epoxy:

$$R_0 = [(1 - n_{e,r})/(1 + n_{e,r})]^2 \approx 0.053. \quad (1)$$

After passing through the surface, the beam undergoes multiple scatterings with the fibers. Since these are qualitatively different for carbon and fused silica, we proceed to discuss the two cases in turn.

3. Carbon Fiber Composite

a. Scattering

Scattering from carbon is quite absorptive, since the index of refraction has a substantial imaginary part at optical and near-infrared wavelengths. A summary of the data is given in [6], and the data are plotted versus wavelength in Fig. 2. At 0.8 μm, for example, we interpolate $n_c = 3.08 + 1.88i$ for the carbon index of refraction. The apparent irregularities in the data near 0.6 and 1.1 μm may be due to the differing systematics of juxtaposed experiments.

Figure 3 shows the absorptivity, as a function of angle of incidence, for 0.8 μm light in epoxy incident on carbon. This is calculated from the Fresnel formulas with a complex index. At normal incidence, the absorptivity is 0.78, while at 45° it is 0.65 (s) or 0.88 (p). Also shown in this figure are the absorptivities versus wavelength, at an angle of 45°. These gradually decrease, with that for p polarization about 0.2 greater than that for s.

When a ray encounters a carbon fiber, the power transmitted into the fiber is assumed to be completely absorbed, since the absorption length in carbon, $l_a = \lambda/[2\pi\ \mathrm{Im}(n_c)]$, is much smaller than the radius. At a wavelength of 0.8 μm, for example, the absorption length is 0.07 μm, as compared with a nominal fiber radius of 5 μm. In our ray-tracing, we follow only the reflected ray, with an appropriately diminished power.

The negative curvature of the fiber surfaces produces a divergence of the ray trajectories. Therefore we expect that a ray will become quickly randomized in direction after a few scatterings. This is illustrated in Fig. 4, which shows representative rays. Note the great variety of ray directions. As a result, the specific positions of the fibers do not appreciably affect the results, justifying our model. The paucity of rays near the bottom shows that almost all of the

power is absorbed within the first few rows of fibers. In our model, rays reaching the lowest surface are absorbed.

To arrive at a reasonable number of rows for the carbon-fiber case, we experimented with 3, 4, and 5 rows. For rays with s polarization, the fraction of power absorbed on the lowest surface decreased geometrically from 0.3% to 0.02%. For p polarization, the absorption was about an order of magnitude lower, depending on the configuration. We settled on 5 rows, guaranteeing less than 0.1% absorption at the bottom.

b. Overall Absorptivity

The single most prominent property of the composite material is its overall absorptivity. This is expected to be somewhat larger for p polarization than for s polarization. It is also expected to fluctuate slightly from run to run, because of the randomized positions of the fibers. These features are borne out by Fig. 5, which shows the results for 40 configurations, at a wavelength of 0.8 μm and a fill factor of 0.5. The absorptivities fluctuate around values of about 0.87 for s and 0.88 for p polarization, with a standard deviation of 0.004.

These values are well above the absorptivity for a single scattering from carbon, shown in Fig. 3. This is a consequence of the multiple scatterings. Note also that the s and p absorptivities of Fig. 5 tend to be closer to one another than for a single scattering. The reason is that a ray with s polarization tends to undergo more scatterings than a ray with p polarization. Thus the difference in path length partially compensates for the difference in single-scattering absorptivities.

Next, the overall absorptivity was calculated for various wavelengths, ranging from 0.5 μm to 4 μm, thus including doubled YAG, regular YAG, COIL (1.3 μm), HF (2.8 μm), and DF (3.8 μm). The results are tabulated in Table 1 and plotted in Fig. 6. In general, the absorptivity decreases slowly from about 0.9 to somewhat less than 0.8. The results for p polarization again exceed those for s, as expected. Note that the difference between p and s absorptivities increases with wavelength.

Table 1: Overall absorptivity of carbon-fiber composite versus wavelength

Wavelength (μm)	Absorptivity (s)	Absorptivity (p)
0.53	0.90	0.91
0.8	0.87	0.88
1.06	0.86	0.88
1.3	0.84	0.86
2.0	0.80	0.83
2.8	0.77	0.81
3.8	0.74	0.79

In the literature, the most relevant measurement appears to be the overall reflectivity of a fiber carbon phenolic at 1.3 μm [1]. Near room temperature, this corresponds to an absorptivity of 0.93, as compared with our nominal value of about 0.85. Since the experimental fiber/epoxy relative volume, and the fiber orientation are not known, we are encouraged by the qualitative agreement.

c. Angular Distributions

We determined the angular distribution of reflected light by monitoring the angles of individual rays emerging (or directly reflected) from the epoxy. The distribution had two components: a large specular peak at near-zero angles, due primarily to reflection from the epoxy, and a diffuse fall-off at other angles, due to multiple reflections from the fibers. The specular component of the reflectivity (about 0.054 for p, 0.055 for s) was slightly higher than the surface reflectivity 0.053, because an occasional ray penetrated the surface and suffered a back-reflection from a fiber. The diffuse component of the angular distribution, shown in Fig. 7, had an approximate cosine dependence on the angle (the expected Lambertian distribution). Thus the reflection into a small surface area at a large distance was roughly isotropic, resulting from directional randomization within the epoxy. The total reflectivities were consistent with the absorptivities noted above.

d. Enhancement

Because of multiple reflections from the fibers, the rays in the epoxy become more densely packed in regions near the surface, as was seen in Fig. 4. Consequently, the optical energy becomes locally enhanced with respect to that of the incident intensity, strengthening the interactions with the epoxy.

Within a given volume element V_i (working temporarily in 3D), the energy density associated with a particular ray *r* is proportional to the power of the ray and the time to traverse the element, divided by the volume of the element, i.e.

$$u_{ir} = n_i P_{ir} l_{ir} /(c V_i), \quad (2)$$

where the index of refraction n_i accounts for the group velocity of light. On the other hand, the energy density associated with the incident flux just within the composite is

$$u_0 = (1 - R_0) n_e P_0 /(c A_0). \quad (3)$$

Here R_0 is the surface reflectivity of Eq. (1), n_e is the epoxy index of refraction, and A_0 is the area illuminated by the beam. The local enhancement is the ratio of the last two quantities, summed over rays. Reverting to two dimensions, we have

$$f_i = \frac{n_i L_0}{(1 - R_0) n_e P_0 A_i} \sum_r P_{ir} l_{ir}, \quad (4)$$

where L_0 is the width of the beam and A_i is the area of the element. In spite of this straightforward definition, the enhancement turns out to be surprisingly complicated to compute within the ray-trace code. We calculate it by setting up a detailed script which runs in conjunction with the code.

Figure 8 shows the energy enhancement computed for a sample configuration, for both s and p polarizations. In each case, the high-enhancement region begins at the surface and extends downward between the fibers in the first row (since the fibers are assumed to be completely absorbing, no enhancement is calculated within them). The maximum enhancement is greater for s polarization (1.6) than for p polarization (1.3). This is as anticipated, since the former case has less absorption and therefore more scattering. With another configuration, the patterns would vary somewhat. However, one would expect nearly the same maximum enhancements.

In Fig. 9 we show the average of the enhancement, as a function of depth. The average is taken along lines parallel to the surface. As expected, the average is somewhat greater for s polarization than for p polarization. The intensification is not high due to the strong absorption in the fibers.

4. Fused-Silica Fiber Composite

a. Scattering

The principal difference between fused silica and carbon is that fused silica is transparent at the main wavelength of interest (0.8 μm). Thus the radiation extends much more deeply into the material, as it is limited only by absorption in epoxy. In the calculations below we assume an epoxy absorption length of 2 mm.The results are insensitive to the specific absorption value if the absorption is small

The index of refraction n_g of fused silica at 0.8 μm is about 1.453 [7], with negligible absorption. Since this is smaller than the index for epoxy, a ray striking a fiber is totally reflected when its angle of incidence is greater than the TIR angle of $\theta_0 = 65.3^o$. The Fresnel transmission from epoxy into fused silica is plotted as a function of angle in Fig. 10. Roughly speaking, rays striking a fiber with angles less than about 60^o are completely transmitted, while rays with angles greater than this are completely reflected. Also shown in this figure is the transmission for rays incident on the fiber/epoxy surface from inside the fiber. This is nearly total for angles less than about 60^o.

Consequently, for incident angles θ less than about 60^o, the path with highest power of a typical incident ray passes once through the fiber, as illustrated in the left-hand plot of Fig. 11. The net scattering angle is $2(\theta' - \theta)$ where θ' is the transmitted angle in fused silica ($n_e \sin\theta = n_g \sin\theta'$). Since the two indices of refraction are comparable, the scattering is rather slight. For example, a ray arriving at 30^o to the normal is scattered by only 6.8^o. This would increase for a larger ratio of indices n_e/n_g.

It should be pointed out that the ray-tracing code follows not only the path of greatest power but also paths with lesser power, within prescribed limits. When the power on a particular ray decreases by a factor of 10^5, the ray is dropped from the calculation.

As an example of multiple scattering from a single fiber, the right-hand plot of Fig. 11 illustrates the scattering which would result if the ratio of fiber/background indices of refraction were considerably smaller than the case considered here. Note the multiple reflected rays.

b. Absorption and Enhancement

A typical geometry for the fused silica composite is shown in Fig. 12. Since the light penetrates deeply into the material, 20 rows of fibers are included. The fiber radius (5 μm) and the relative fiber/epoxy areas (50/50) were the same as in the carbon-fiber case.

Figure 13 shows the local enhancement pattern calculated for this geometry. This is for p polarization, but the case with s polarization is not much different. The maximum is about 2.1. The relatively small intensification is related to the small difference in refractive indices of the fiber and matrix. Of the incident power, about 12% was reflected, with more than half of this in diffusive components. The fraction absorbed at the bottom was 72%. Thus about 16% was absorbed by the epoxy.

Figure 14 shows the average enhancement (as averaged over the direction parallel to the surface) versus depth. This consists of successive narrow peaks and valleys, corresponding respectively to the space between rows of fibers and the fibers themselves. The maximum value of about 1.5 is reached just before at about 98 μm (just before the ninth row). This pattern is typical for propagation in turbid media [2]. Field intensification is related to the slowdown of propagation in the material, and the intensity decrease near the boundary is explained by the radiation losses via backscattered light.

5. Connection with Macroscopic Model

In the previous sections, we developed a microscopic model for light propagation in a composite material. As a first-principles approach, it is quite expensive computationally (and this would be exacerbated in 3D geometry). On the other hand, there also exist some simple macroscopic models describing radiation transport in scattering media [2,3]. Here we will use a two-flux model which is extensively employed in industry and which provides a good description of experiments [4].

In the two-flux model, the radiation is divided into two fluxes. One flux (F_+) propagates in the direction of the incident radiation, and the other flux (F_-) propagates in the opposite direction. The steady-state equations describing light propagation are [2]:

$$\frac{dF_+}{dz} = -(K+S)F_+ + SF_- , \quad \frac{dF_-}{dz} = (K+S)F_- - SF_+ . \qquad (5)$$

Here the positive constants *K* and *S* describe the damping and scattering, respectively, of radiation. These equations are to be solved in a slab of thickness *h*. They are subject to the boundary conditions:

$$F_+(0) = F_0, \quad F_-(h) = 0. \qquad (6)$$

These state that just within the slab, the positive-flowing flux equals the incident flux F_0, and that at the opposite end, the backward-flowing flux vanishes.

Each of the fluxes is found to consist of two terms, one varying as $\exp(-pz)$ and the other as $\exp(pz)$, with $p = +[K(K+2S)]^{1/2}$. From the solution, we find that the transmitted flux $F_+(h)$ and the reflected flux $F_-(0)$ are given by:

$$F_+(h) = F_0 \frac{(a^2-1)b}{a^2b^2-1}, \quad F_-(0) = F_0 \frac{a(b^2-1)}{a^2b^2-1}, \qquad (7)$$

where

$$a = (K+2S+p)/(K+2S-p), \quad b = \exp(ph). \qquad (8)$$

Conversely, if we know the transmission coefficient $T = F_+(h)/F_0$ and the reflection coefficient $R = F_-(0)/F_0$, then we can deduce the constants *K* and *S* in the governing equations via:

$$K = \frac{(a'-1)\ln b'}{(a'+1)h}, \quad S = \frac{2a'\ln b'}{(a'^2-1)h}, \qquad (9)$$

where

$$\begin{aligned} a' &= (1+R^2-T^2+[(1+R^2-T^2)^2-4R^2]^{1/2})/2R, \\ b' &= (1-R^2+T^2+[(1+R^2-T^2)^2-4R^2]^{1/2})/2T. \end{aligned} \qquad (10)$$

Within our ray-tracing model, we can find the average *z*-dependence by averaging the enhancement over *x*. Using the calculated transmission and reflection, we can then solve for the distribution of the light inside the sample, according to the two flux model.

The results for the fused silica fibers case are shown in Fig. 14. Here we have used, from the previous ray-tracing results for fused silica, a transmission coefficient of 0.7 and a reflection coefficient of 0.07 (in the latter, the incident reflectivity has been subtracted). Because of problems caused by scattered light near the surface, which are common to all macroscopic models [2], we have applied an overall normalization to the two-flux solution. Beyond a narrow layer near the surface, we observe a good description of the behavior of the average flux.The drop of the intensity near the surface due to the scattering losses is not described by the two-flux

model.[2] The damping and scattering coefficients, or rather their inverses, follow from Eqs. (9) and (10) as $K^{-1} =$ 950 μm and $S^{-1} = 2600$ μm.

We note that the above procedure is similar to the experimental approach to the measurements of the parameters K and S [2,7].

6. Summary and Conclusions

We have developed a detailed ray-trace model which can be used to calculate the absorptivity and energy enhancement of composite materials, starting with the optical parameters of the constituents and the material structure. These will serve as components of a comprehensive model of composite behavior under the effects of laser radiation.

The ray-trace model is sufficient for the description of carbon-based composites, for which absorption occurs relatively near the surface. We have presented calculations of the absorptivity of the composite material for different frequencies of incident radiation, as well as of the energy enhancement.

For the glass fiber-based composites, light penetrates much more deeply. Here calculations with the ray-trace model are still valid but are more time-consuming. We have shown that this model is usefully supplemented by a macroscopic two-flux model, which utilizes parameters obtained from the ray-trace code. Thus we are able to bridge the gap between microscopic and macroscopic descriptions of composite materials.

Our approach to the study of light propagation in composite materials can also be extended to other translucent materials and to paint. It is straightforward to change the material, fiber orientation, and size. In the case of the paint, instead of fibers the scattering is produced by small particles, which can be easily incorporated into the model. Our approach can be utilized to calculate the energy deposition in the material, and it should be a part of a predictive thermo-mechanical description of material behavior under the effects of high-power laser radiation.

Acknowledgments

This work performed under the auspices of the U.S. Department of Energy by Lawrence Livermore National Laboratory under Contract DE-AC52-07NA27344.

References

1. R. K. Freeman, F. A. Rigby, and N. Morley, "Temperature-Dependent Reflectance of Plated Metals and Composite Materials Under Laser Irradiation," J. Thermophys. and Heat Transfer **14**, 305-312 (2000).

2. A. Ishimaru, *Wave Propagation and Scattering in Random Media* (Academic Press, 1978).

3. Ya. B. Zeldovich and Yu. P. Raizer, *Physics of Shock Waves and High Temperature Hydrodynamic Phenomena*, Academic Press, NY, 1967.

4. P. Mudgett and L. Richards, "Multiple Scattering Calculations for Technology," Appl. Opt. **10**, 1485-1502, 1971.

5. Our ray-tracing utilizes the application FRED, distributed by Photon Engineering, LLC, Tucson, AZ.

6. A. Borghesi and G. Guizzetti, "Graphite (C)," in *Handbook of Optical Constants of Solids*, Vol. II, E. D. Palik, ed. (Academic Press, 1981), pp. 449-468.

7. W. L. Wolfe and G. J. Zissis, *The Infrared Handbook*, Infrared Information Analysis Center, 1985.

Figure Captions

1. Schematic geometry of the carbon-fiber model. The fibers, seen head-on, are first arranged in uniform rows and then slightly perturbed. The two mirrors account for the limited extent of the beam. The fibers, or portions of them, outside the mirrors are not included in the ray-tracing.

2. Left: index of refraction of carbon (graphite, ordinary mode) versus wavelengths, from data given in [6]. Upper blue line: real part; lower red line: imaginary part.

3. Fresnel absorptivity of 0.8 μm light incident on carbon from epoxy. Top: angular dependence at 0.8 μm. Bottom: wavelength dependence at 45^{o}.

4. Sample rays within the epoxy, with carbon fibers, after several steps. (In a step, each ray advances from one surface to the next.) The pattern at the top indicates reflected rays.

5. Calculated absorptivity of the carbon-fiber composite, at a wavelength of 0.8 μm, for 40 fiber configurations. Upper points: p polarization; lower points: s polarization. The dotted lines give the averages (about 0.88 and 0.87, respectively). Each run involved 10^6 laser rays. Note that the vertical scale is truncated.

6. Calculated absorptivity of the carbon-fiber composite versus wavelength. Each point represents an average over 10 configurations, with 10^6 laser rays each. The jump near 1 μm is caused by the apparent irregularity in the graphite index of refraction in Fig. 2.

7. Calculated angular distributions of light reflected from the carbon-fiber composite, away from the specular (backwards) direction. The jagged lines show the computed results, while the dotted lines give the best fit to a function proportional to $\cos\theta$. The curves are normalized so that the integral gives the total diffuse reflectivity.

8. Local enhancement for a particular carbon-fiber configuration. Top: s polarization; bottom: p polarization. Note the shadows produced by the first row of fibers.

9. Average enhancement versus depth, for the distributions of the previous figure.
10. Left: Fresnel transmission of 0.8 μm light incident from epoxy onto fused silica. Right: transmission for incidence from fused silica onto epoxy.

11. Left: Dominant scattering of a sample ray from fused silica. The incident ray arrives at $\theta = 30^{o}$ normal to the surface, and the outgoing ray is diverted from the path traveled by the incoming normal ray by a net angle of $\delta\theta = 6.8^{o}$. Right: Example of scattering in a system with a smaller ratio of fiber/background indices of refraction. Note the multiple reflections and the sequence of interior isosceles triangles.

12. Typical geometry of the fused-silica composite model.

13. Local enhancement for fused silica fibers. The maximum enhancement is 2.1. The null areas (blue) along the sides indicate areas in which the enhancement was not calculated, due to complications caused by reflections.

14. Average enhancement versus depth, for the distribution of the previous figure. The dashed line shows the result from the two-flux model.

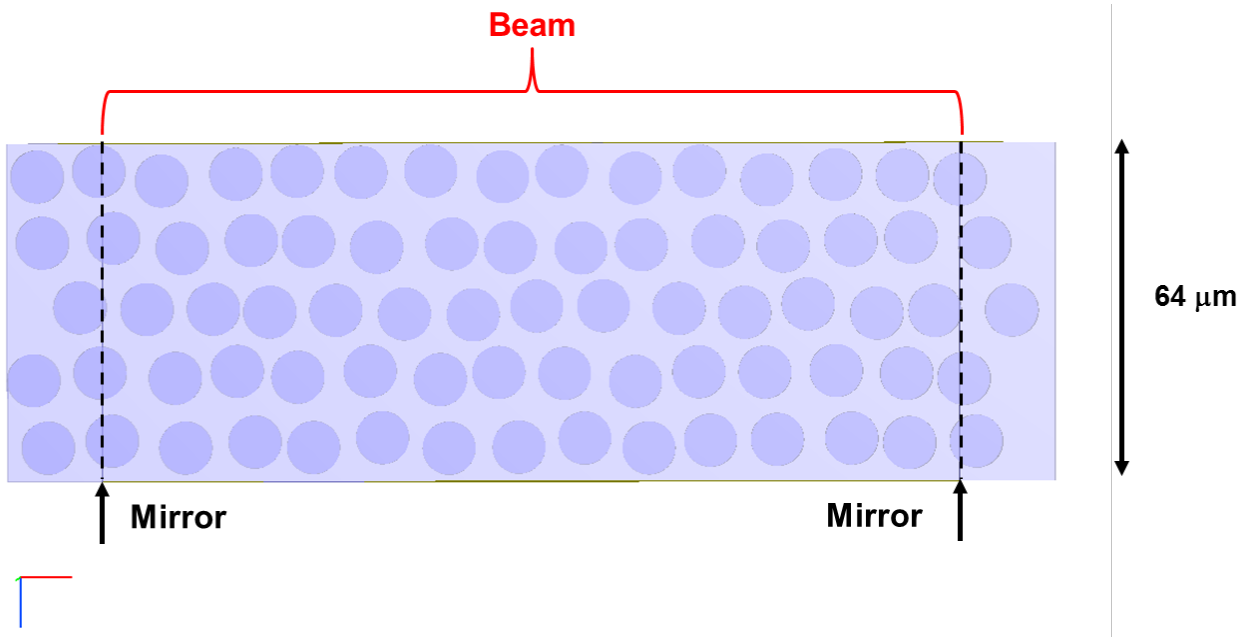

Fig. 1

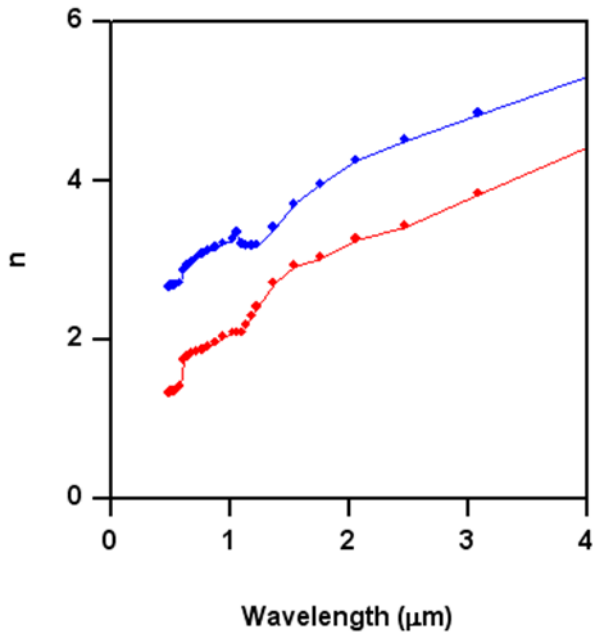

Fig. 2

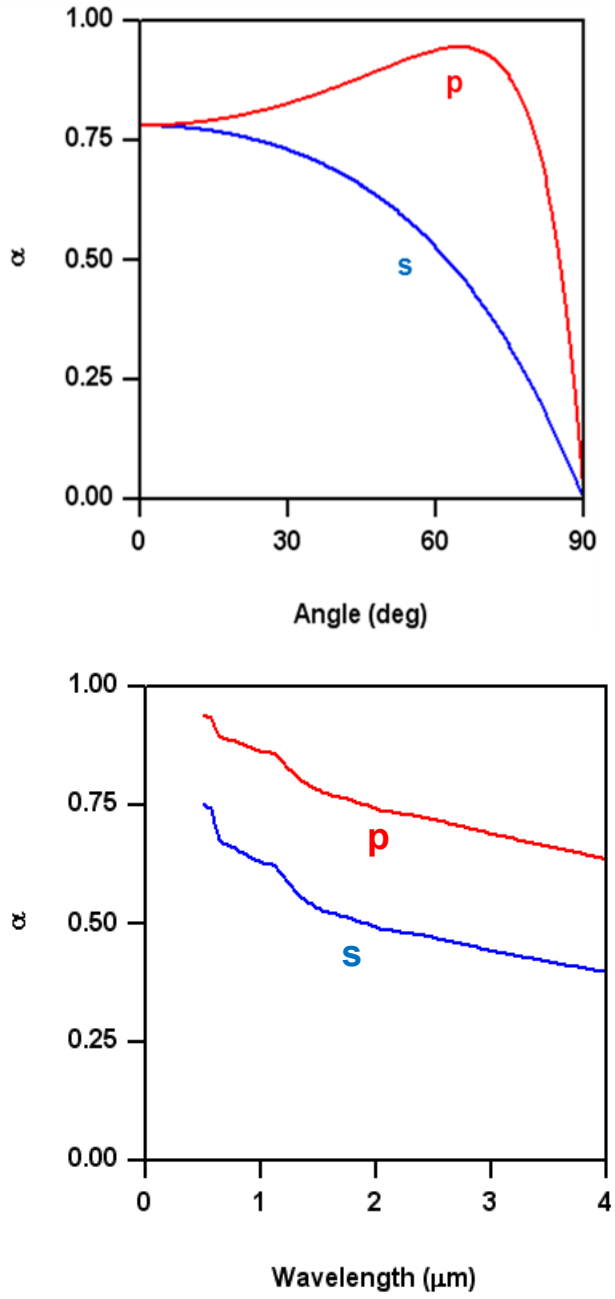
1.00
0.75
0.50
0.25
0.00
α
p
s
0
30
60
90
Angle (deg)
1.00
0.75
0.50
0.25
0.00
α
p
s
0
1
2
3
4
Wavelength (μm)

Fig. 3

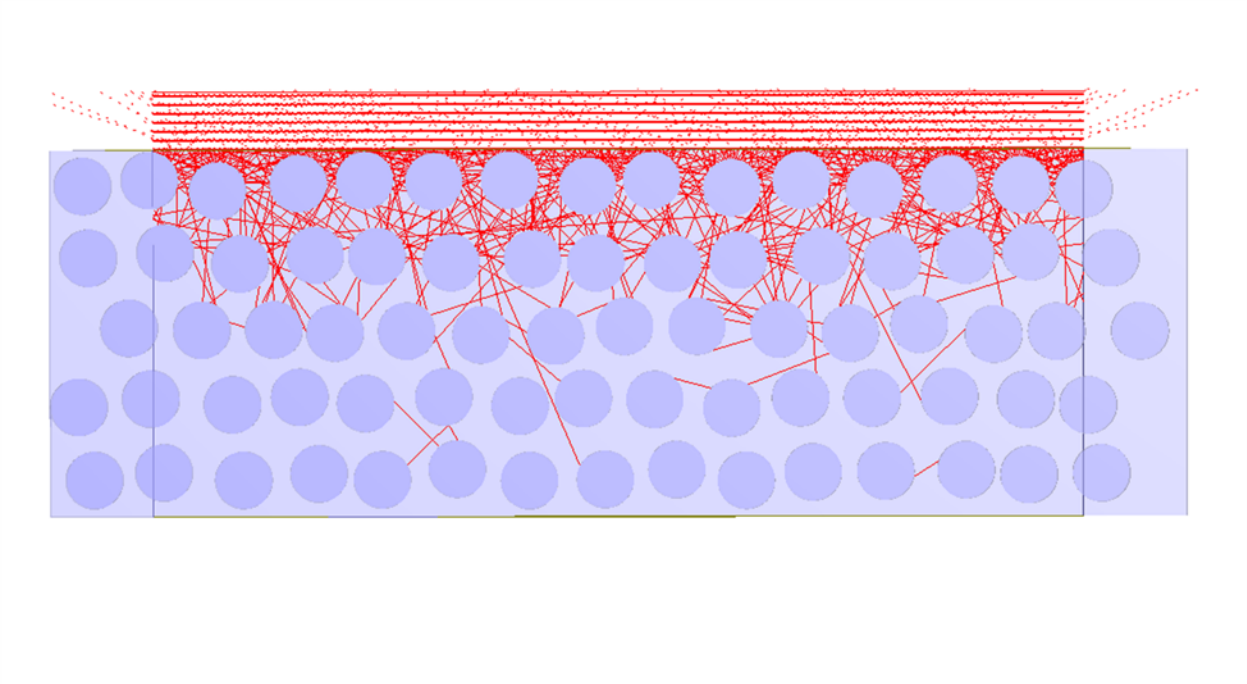

Fig. 4

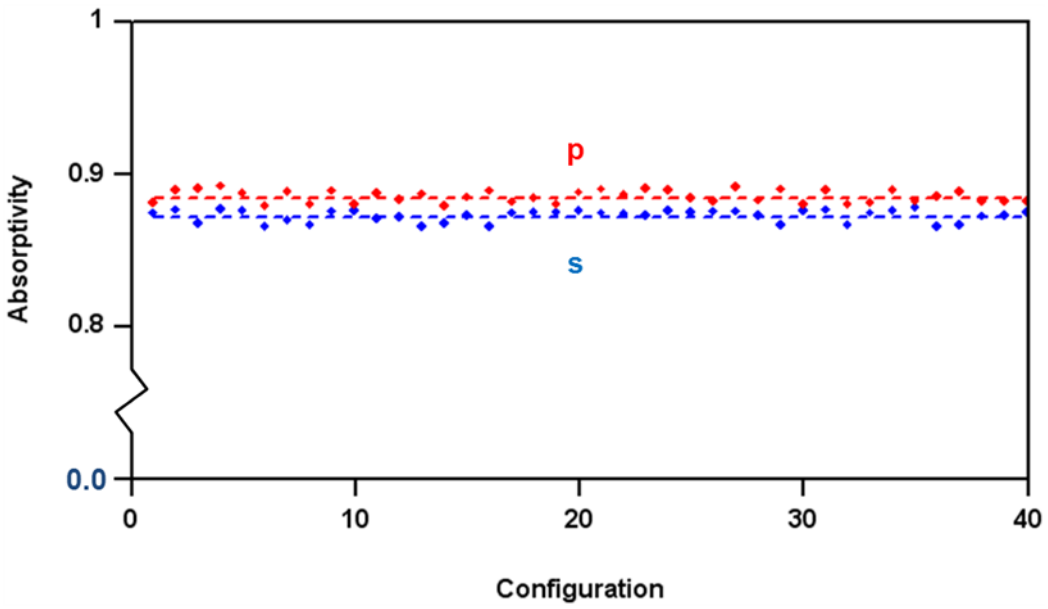

Fig. 5

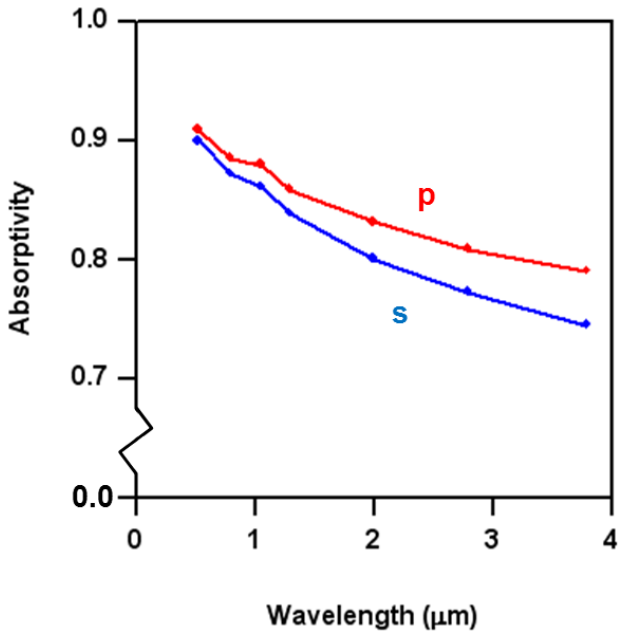

Fig. 6

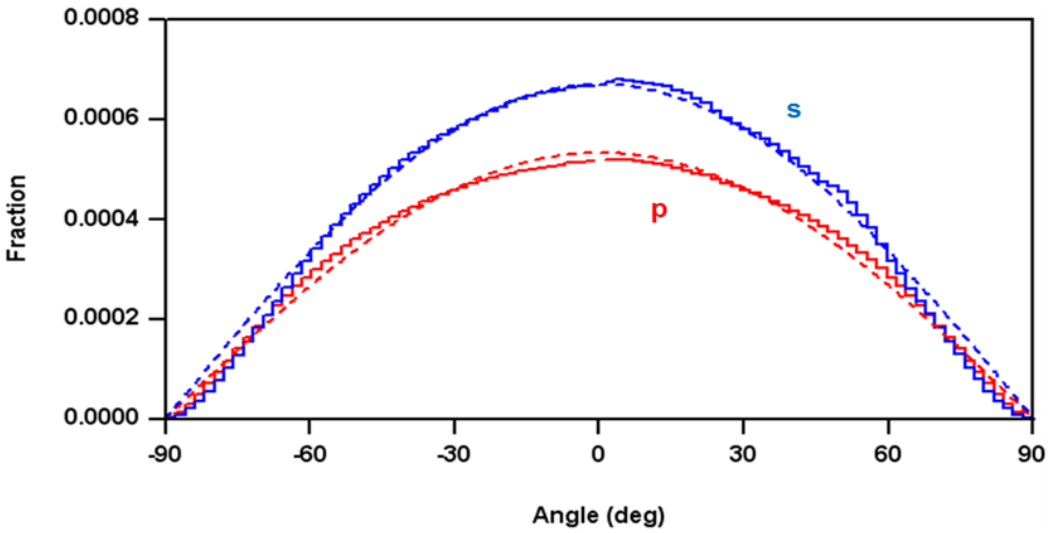
0.0008
0.0006
0.0004
0.0002
0.0000
Fraction
s
p
-90
-60
-30
0
30
60
90
Angle (deg)

Fig. 7

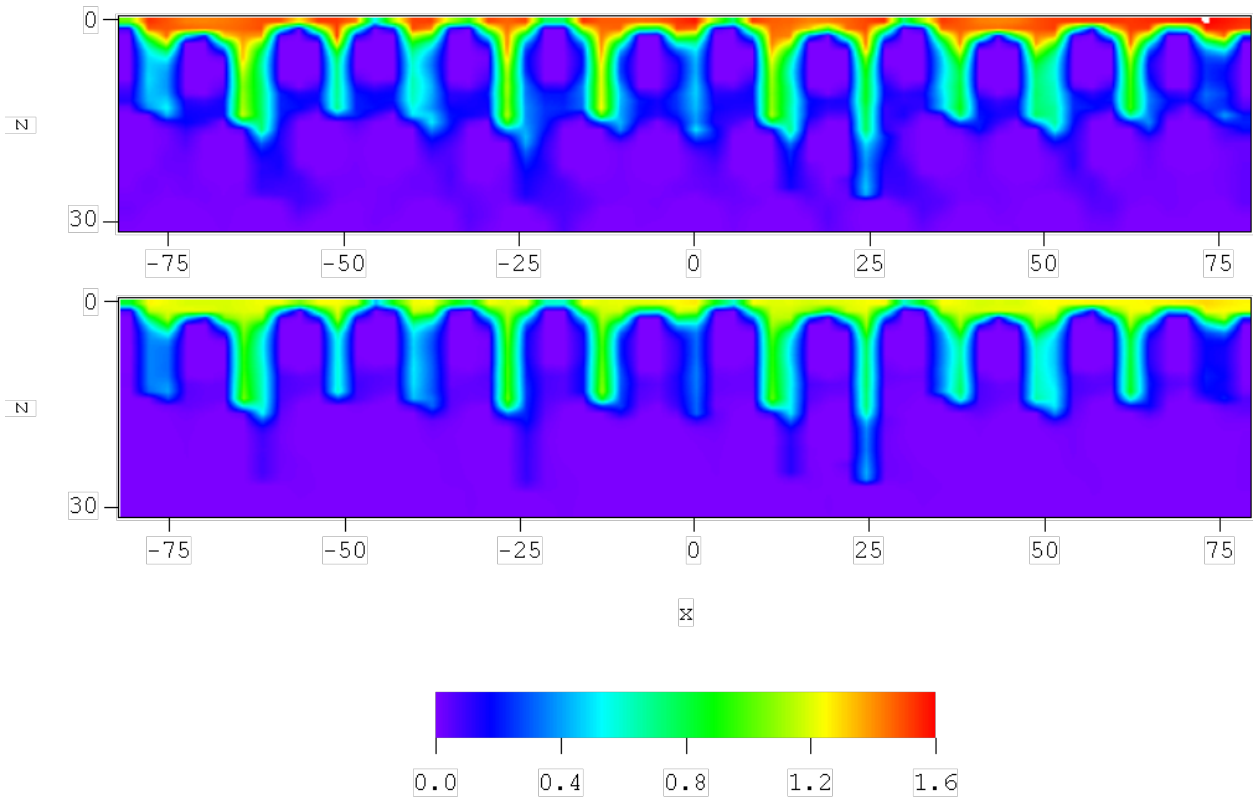

Fig. 8

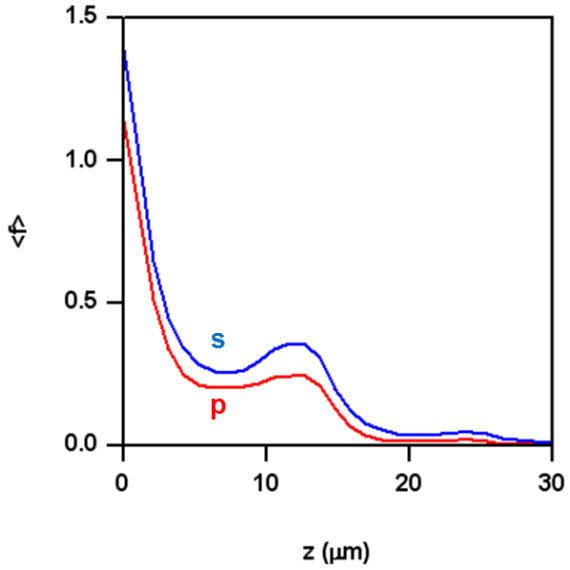

Fig. 9

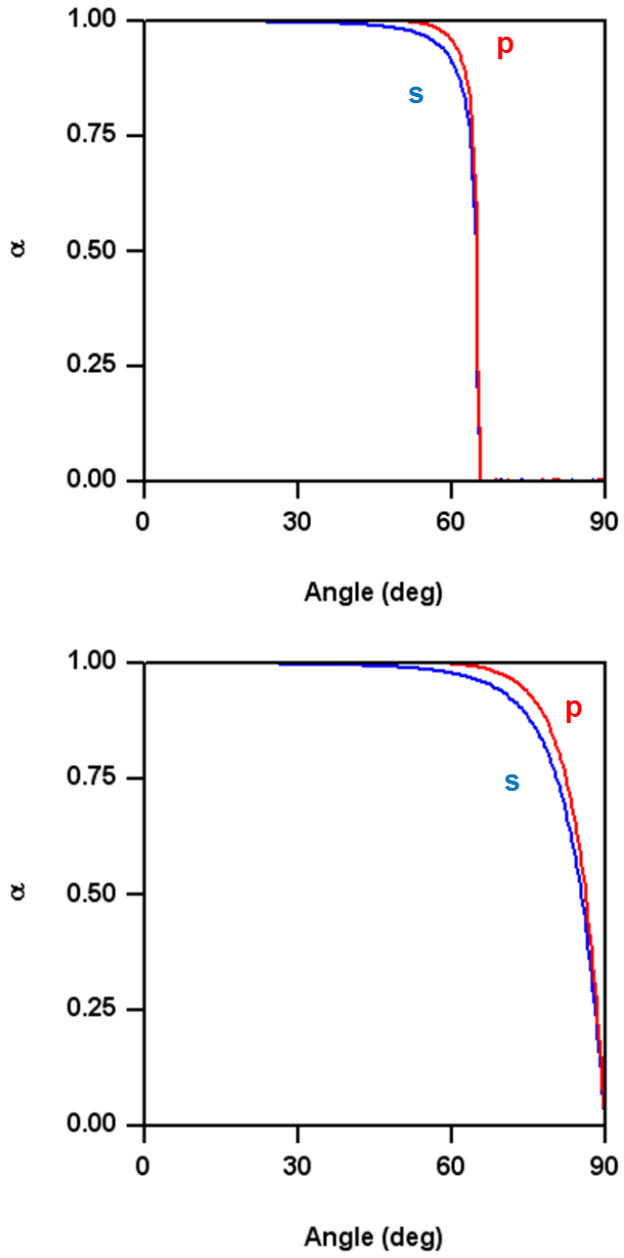
1.00
0.75
0.50
0.25
0.00
α
0
30
60
90
Angle (deg)
p
s
1.00
0.75
0.50
0.25
0.00
α
0
30
60
90
Angle (deg)
p
s

Fig. 10

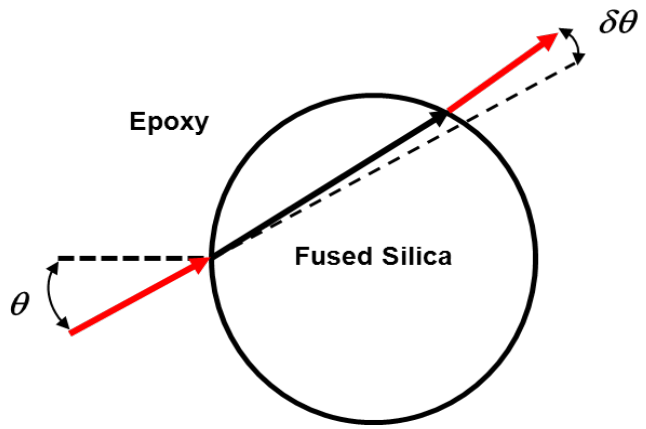

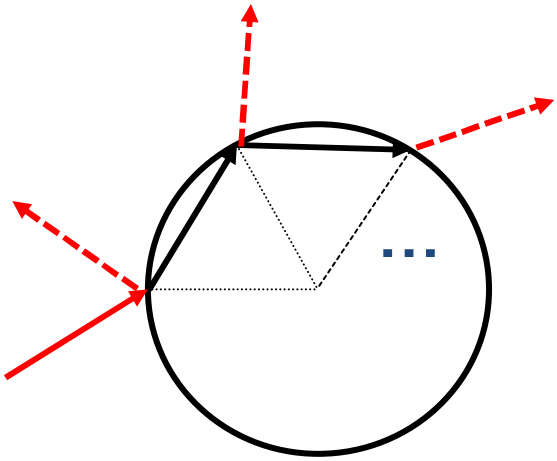

Fig. 11

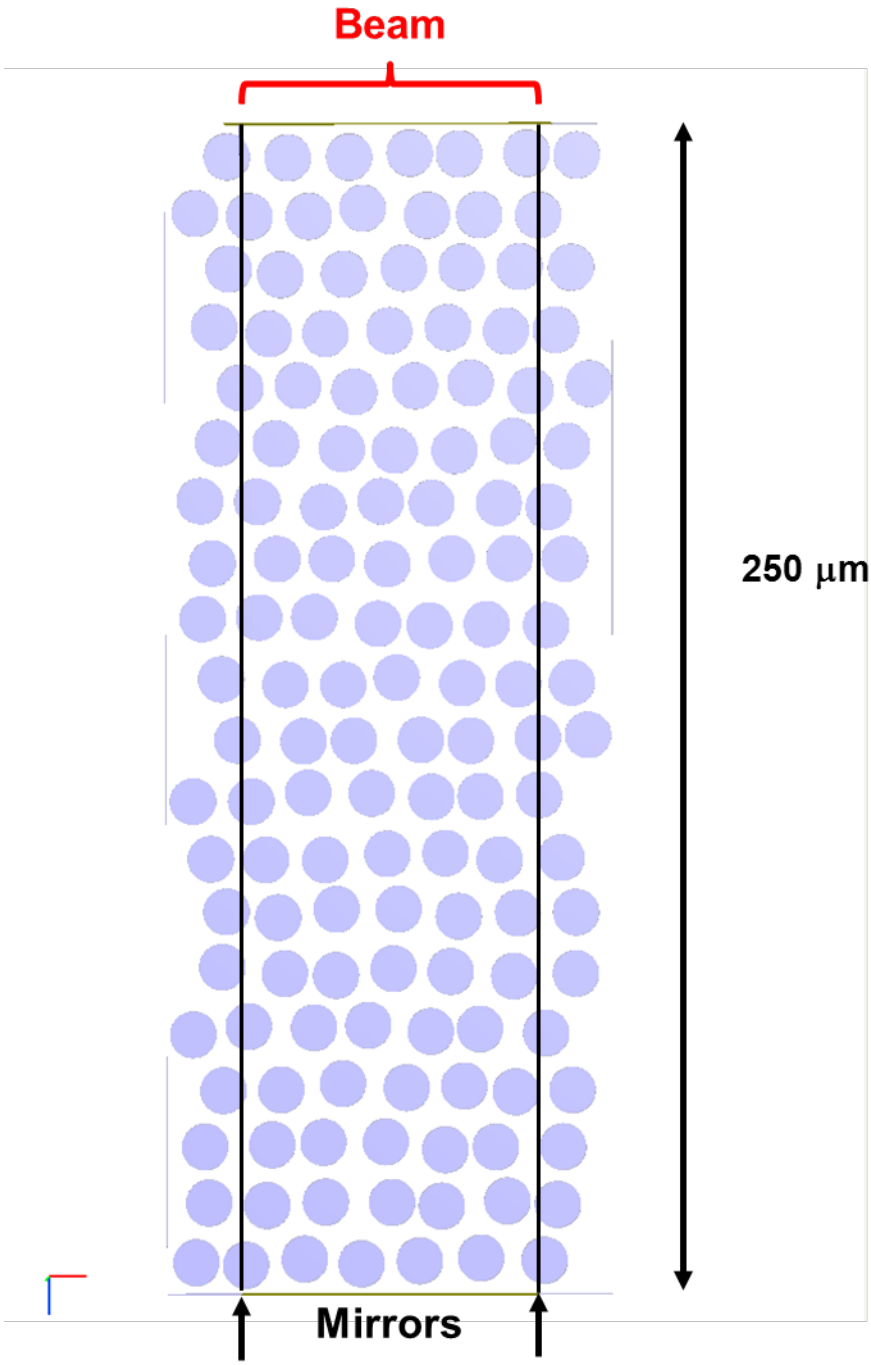

Fig. 12

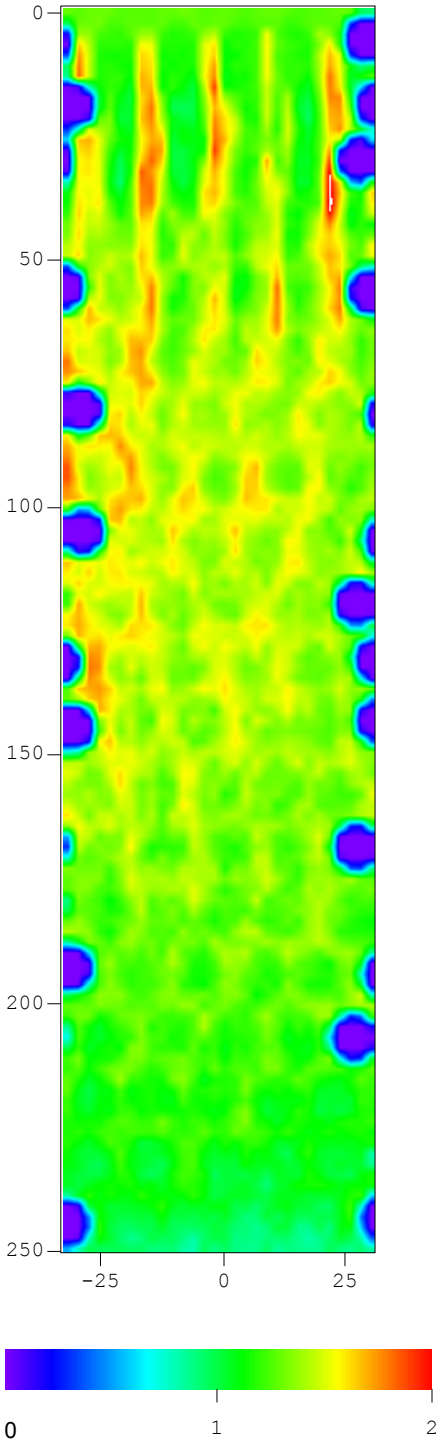

Fig. 13

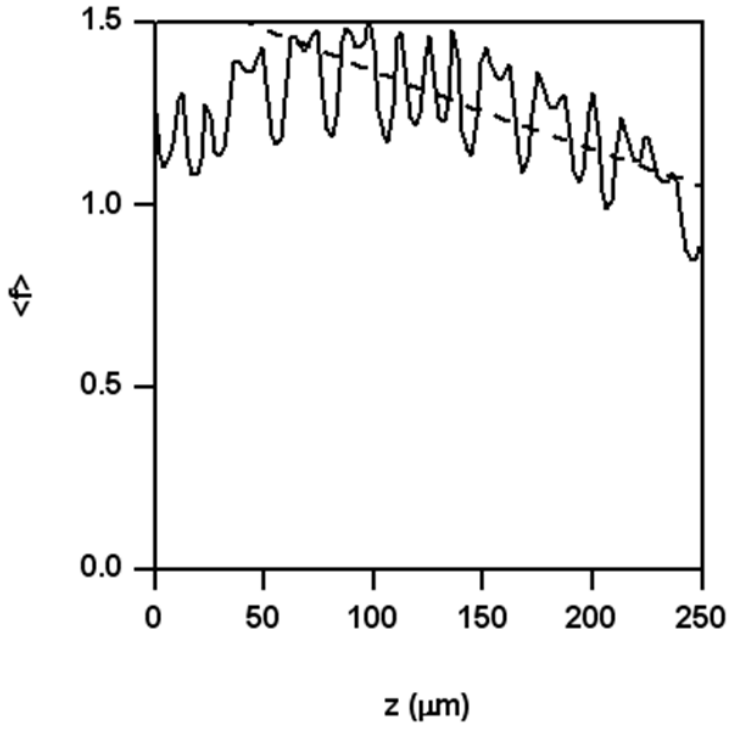

Fig. 14